Korean J. Chem. Eng., **26**(2), 339-348 (2009)

Evaluation of jet performance in drop-on-demand (DOD) inkjet printing

Byoung Wook Jo, Ayoung Lee, Kyung Hyun Ahn†, and Seung Jong Lee

School of Chemical and Biological Engineering, Seoul National University, Seoul 151-744, Korea
(*Received 8 June 2008 • accepted 18 August 2008*)

Abstract−Inkjet printing has been widely used in many applications and has been studied for many years. However, there are not many systematic researches on the mechanism of jet formation, nor is there any reliable platform that enables us to evaluate jet performance. In this study, an approach to practically evaluate the jet stability of the drop-on-demand (DOD) inkjet printing has been proposed, based on which the transient behavior of the DOD drop formation has been studied experimentally for Newtonian liquids with a range of different viscosities (1.0-11 cp) but of a comparable surface tension. For more viscous liquids, the rate of the jet retraction after a pinch-off from the nozzle was found to increase as the thread motion became more sharp and conical as a result of the shape effect. The break-up time of the jet also increased because the rate of capillary wave propagation was lower for more viscous liquids. The jet stability graph, which can be drawn in terms of jet retraction and break-up time, was employed to characterize the jetting stability, and the degree of satellite drop generation was quantitatively evaluated by two critical jet speeds. The effect of an electric pulse imposed on a piezoelectric plate inside the printhead was also studied. The single-peak electric pulse was used in this experiment for simple analysis, and the jet speed variation was measured under different operating conditions. Both the optimal dwell time and the maximum stable jetting frequency were affected by viscosity and they were explained in terms of the propagation theory.

Key words: Drop-on-demand, Inkjet Printing, Drop, Viscosity, Jetting Stability, Jetting Window

INTRODUCTION

With rapid advances in information technology (IT), coating and printing processes that mark fine and clear patterns on the substrate are getting more attention. The drop-on-demand (DOD) inkjet printing technology, for example, is now being recognized as a promising tool in this area. It is because the inkjet printing has the advantage of making patterns without any additional lithographic processes. Inkjet printing can reduce the number of processing steps compared with conventional patterning processes, and it finally results in a lower production cost in manufacturing. For this reason, many approaches to substitute the conventional coating method with inkjet printing are in progress. Examples include color filter coating in flat panel display (FPD), electric wire coating on printed circuit board (PCB), UV-curable resins for the fabrication of micro-optical parts, polymer light emitting diode (PLED) displays and so on [1-6].

New application of inkjet printing requires advances not only in new ink and equipment but also in understanding the mechanism of ink drop generation. It is essential to get a clear comprehension on how the liquid properties such as viscosity, surface tension, and elasticity affect the jetting stability. There are a few studies on the jet formation of polymer solutions, according to which a significantly different drop formation can be observed when the high molecular weight (MW) polymer is added. Mun et al. [7] studied the viscoelastic jet formation using glycerol/water mixtures in which poly(ethylene oxide) (PEO) of different MW was added, and showed the formation of beads-on-a-string structure when a high MW polymer was added. Using the same polymer, Christanti and Walker [8,9] showed that the formation of a thin thread structure is related with the strain hardening behavior of a high MW polymer. The dynamics of viscoelastic jets was also studied by Cooper-White and coworkers [10]. But most of these studies have focused on gravity-driven or continuous flow.

To understand the jetting behavior of the liquids with different viscosity and surface tension, numerical analysis has also been employed [11-16]. In the numerical analysis, it is important to obtain the pressure profile at the nozzle exit generated by the expansion and constriction of the piezoelectric transducer (PZT). Many researchers adopted acoustic wave theory to predict the pressure history. Bogy and Talke [17] introduced a theory to show that the generation of sufficient pressure at the nozzle tip is due to the constructive interference of the acoustic waves inside the printhead tube. This theory was not only used to predict the pressure at the nozzle tip but also to explain the effect of the imposed electric pulse width (dwell time) on the jetting behavior. Using this theory, Wu et al. [18] could obtain the optimal dwell time of DI water and ethylene glycol, which was close to the measured value. Besides the pulse width, the effect of pulse frequency was also studied and explained with regard to the generation and decay of the acoustic waves [17, 19]. However, there are not many studies that experimentally characterize the jetting behavior of the DOD inkjet printing system. Carr et al. [20,21] studied the transient behavior of drop formation. Shore et al. [22] investigated the effect of elasticity on the on-demand drop formation by using low viscous elastic liquids. However, no suggestion has been made to define the jetting stability, which can be one of the yardsticks to define the quality of the ink. One of the important indices to determine the jet stability is to investigate the generation of satellites. Once formed, these satellites can easily lose directionality and deteriorate printing quality. This becomes critical when a very fine pattern is required. In spite of this importance, it is hard to quantitatively define the degree of satellite formation because it

†To whom correspondence should be addressed.
E-mail: ahnnet@snu.ac.kr

is affected by many processing parameters such as the imposed pulse shape and frequency.

Recently Dong et al. [23] investigated the effect of the liquid and system parameters on the recombination of the primary drop and satellites. Based on theoretical approaches, they proposed a necessary condition for the recombination of separated drops and the limit of liquid thread length to avoid a break-up during the jet contraction. But there still exists a limitation that complex fluids such as colloidal suspensions or polymer solutions are too complicated to analyze with the theoretical basis.

In this paper, we investigate drop generation in the DOD inkjet printing and suggest a method to evaluate the jetting performance of a liquid. The jetting window is to be employed to check jettable condition for three different viscous liquids as a function of pulse amplitude and dwell time. Based on the dynamics of jet retraction and break-up, the jet stability graph will be illustrated to explain how the viscosity affects the jetting behavior. It enables us to determine the degree of satellite generation from two critical jet speeds. Finally, the effect of pulse dwell time and frequency on the drop formation will be investigated and the experimental results with different viscous liquids will be discussed by employing the propagation theory.

EXPERIMENTAL SETUP

A schematic of the experimental setup is shown in Fig. 1. The printhead consists of an ink supply connector, a printhead tube and a glass nozzle. At the tip of the glass nozzle, a 50 μm size pore through which the drop can be ejected is punctuated.

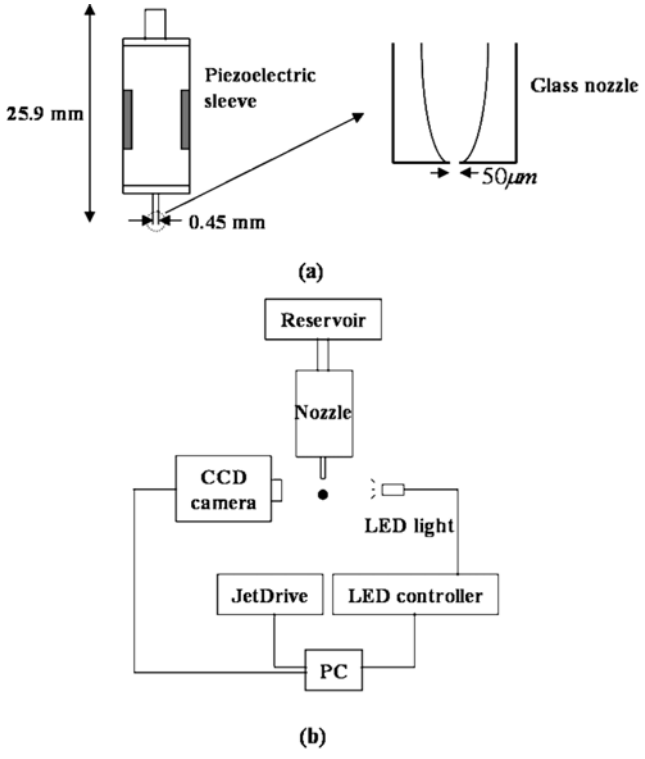

Fig. 1. Schematic of the inkjet system: (a) geometry of the inkjet printhead, (b) a schematic diagram of the experimental apparatus.

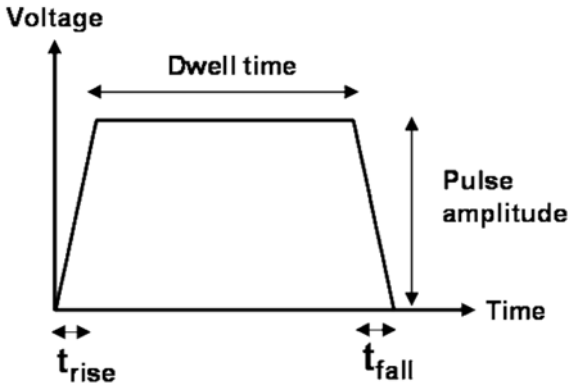

Fig. 2. Typical profile of a single-peak electric pulse. The imposed voltage to piezoelectric transducer is the pulse amplitude and the imposing time of a pulse is called dwell time.

Fig. 3. An illustrative sequence of DOD inkjet drop formation.

The electric pulse made by JetDriveIII (MicroFab) is applied to the piezoelectric transducer (PZT) in the printhead tube. To simply understand how the pulse shape affects the drop formation, a single-peak pulse pattern is used in this experiment, although echo time is another parameter to contribute the drop stability (Fig. 2). The rising time, t_{rise} and the falling time, t_{fall} are fixed at 3 μs, which satisfies the requirement for the proper jet formation [18]. This pulse makes the piezoceramic plates deform periodically and generate an acoustic wave in the liquid.

If this wave is amplified by resonance at proper conditions, the liquid can spurt out of the nozzle. The typical behavior of an ejected drop is shown in Fig. 3. A CCD camera (HR-50, Sony) is used to get these images. To capture the images of a fast moving liquid drop, a stroboscopic method is employed, with which we could get the pictures of drop deformation at the time scale of 0.1 microseconds by changing the delay time between the pulse inception and the flash of LED light. As for the reproducibility of drop formation, the piezo-material's maintenance as a component of the nozzle and cleaning of orifice are important factors, and the Newtonian fluids keep clean an orifice compared to non-Newtonian fluids with included polymer and/or particles.

A typical process of drop formation shown in Fig. 3 can be classified by the following steps.

(a) Jet ejection with stretching: a liquid is ejected out of the nozzle. Then the liquid head extends out and the liquid column begins to stretch.

(b) Jet pinch-off from the nozzle: at the nozzle exit, the diameter of the liquid column keeps decreasing and finally pinches off, after which the liquid thread becomes free to move in the air with almost constant velocity.

(c) Jet retraction: after the liquid thread pinches off from the nozzle, the capillary force makes the drop tail move toward the head, which results in drop retraction or recoiling.

Table 1. Shear viscosity and surface tension of prepared samples

Sample	Glycerol (wt%)	DI water (wt%)	Shear viscosity (mPa·s)	Surface tension (mN/m)
A	0	100	1	72
B	20	80	2.8	68
C	40	60	4.7	67
D	60	40	10.9	65

(d) Jet breakup/recombination: During drop retraction, the propagation of capillary wave on the liquid thread causes the separation of the main drop into a primary drop and secondary drops called satellites. Depending on the condition, the satellites may recombine with the primary drop or not.

Newtonian liquid samples used in this study are characterized in Table 1. Glycerol and DI water were mixed in different compositions to change shear viscosity. Glycerol added water solutions have almost the same static surface tension, which is a little lower than that of DI water. Although the drop deformation is regarded as mainly dominated by the dynamic surface tension rather than the static surface tension at the very short period of time, it is not taken into account in this experiment because its effect is known to be less significant [24]. In this sense, we can isolate the effect of viscosity while keeping the surface tension nearly constant.

RESULTS AND DISCUSSION

1. Measurement of Jet Retraction Speed

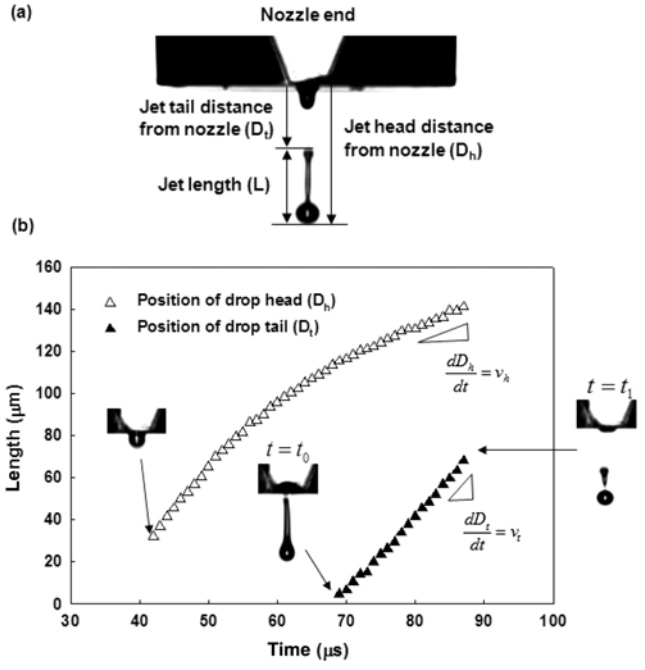

Fig. 4. Transient behavior of the liquid jet: (a) three representative parameters in drop deformation, (b) evolution of jet head distance (D_h) and jet tail distance (D_t) from the nozzle at pulse amplitude 30 V. The slope of the graph after jet pinch off from the nozzle ($t=t_0$) corresponds to the jet head speed and jet tail speed, respectively.

In understanding the drop deformation after ejection, the time variation of the jet head distance (D_h) and tail distance (D_t) from the nozzle (Fig. 4a) are important parameters. In this study, the parameters related to the jet length (L) rather than the jet diameter have been more focused because there is little variation in the width of the jet thread.

The typical time variation of jet thread is shown in Fig. 4b. The distance is measured from 42 μs after the pulse inception. The jet stretches until a pinch-off at 69 μs (t_0), after which the distance of the jet tail is measured until the drop breaks up to form a secondary drop at 88 μs (t_1).

After the pinch-off (t_0), the variation of the jet head and tail position is almost linear with time. Hence the jet head speed (v_h) and jet tail speed (v_t) can be obtained from the slope of the curve. The behavior of these parameters is shown in Fig. 5. Here, the jet retraction speed (v_r) is calculated by using the following relationship:

$$L = D_h - D_t \tag{1}$$

$$v_r = -\frac{dL}{dt} = v_t - v_h \tag{2}$$

It is well known that the jet speed is proportional to the pulse amplitude. On the other hand, the retraction speed is inversely proportional to the pulse amplitude. This is because the jet tail speed (v_t) is not much influenced by the motion of the jet head and stays almost constant, as can be seen in Fig. 5.

Keller [25] analyzed the retreating motion of a breaking thread with a circular cross section of the radius r(x). To solve the momentum equation, he assumed $r(x)=Rx^{\alpha}$ for $x>0$, where R is the constant. α is a kind of input shape factor. For a uniform thread $\alpha=0$, for parabolic thread $\alpha=2$, and for conical thread $\alpha=1$. Then the position of the thread end can be derived as follows:

$$X(t) = t^{2/(2+\alpha)}\left(\frac{\gamma(2\alpha+1)(2+\alpha)^2}{\rho r(3\alpha+2)}\right)^{1/(2+\alpha)}, \tag{3}$$

where γ is the surface tension, ρ is the density. Then, for a uniform

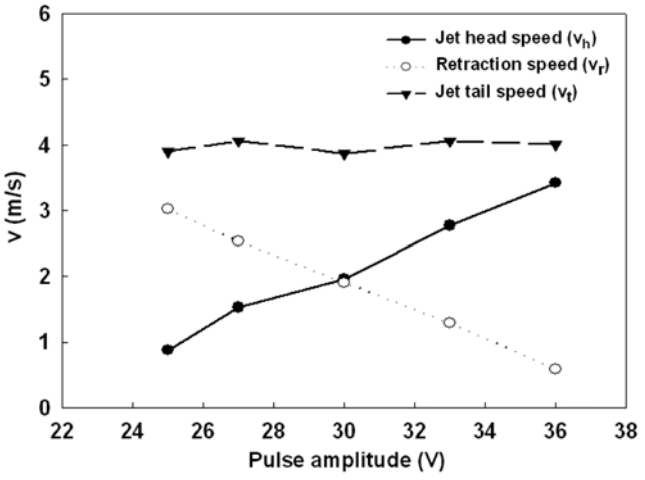

Fig. 5. Jet speed and retraction speed of DI water at different pulse amplitudes. Jet head speed is proportional to the imposed pulse amplitude while jet tail speed remains almost constant. Retraction speed (v_r) is defined as the speed difference between jet head and tail ($v_t - v_h$).

Table 2. Characteristic parameters to determine the jet retraction speed calculated at different pulse amplitudes

Liquid	Voltage (V)	Jet tail speed (V_t) (m/s)	Initial length (L_0) (μm)	Capillary speed v_{ca} (m/s)	v_t/v_{ca}	Re_j	Oh^2
DI water	25	3.8	47	1.70	2.2	180	0.00056
	27	4.2	56		2.5	230	
	30	4.0	73		2.3	290	
	33	4.0	82		2.3	330	
	36	4.0	100		2.3	400	
Glycerol 20 wt%	25	3.6	46	1.61	2.2	61	0.0044
	27	3.3	54		2.1	68	
	30	3.2	70		2.0	84	
	33	3.4	87		2.1	110	
	36	3.5	114		2.2	150	
Glycerol 40 wt%	25	4.4	34	1.55	2.8	35	0.012
	27	4.2	46		2.7	46	
	30	3.9	65		2.5	60	
	33	3.7	82		2.4	72	
	36	3.9	99		2.5	91	
Glycerol 60 wt%	33	5.1	88	1.48	3.4	48	0.06
	36	4.8	102		3.3	53	
	39	4.7	122		3.2	62	
	42	4.7	129		3.2	65	

thread (α=0) and negligible viscous effect, the retraction speed of the thread can be obtained as follows:

$$v_r = \frac{dX(t)}{dt} = \left(\frac{2\gamma}{\rho R}\right)^{1/2}. \quad (4)$$

This means that the end of a broken liquid thread moves with a constant velocity, in the same manner as previously found by Talyer [24] and Culick [26] for the growth of a hole in a uniform film.

Dong et al. [23] referred to jet tail speed (v_t) as a retreating speed (v_{ret}) and estimated it using Keller's equation. They rescaled the thread radius as the radius of the nozzle (R_{noz}) and simplified the retreating speed as follows:

$$v_t \approx a v_{ca}, \quad (5)$$

where a is a constant and v_{ca} is the capillary speed which is $(\gamma/\rho R_{noz})^{1/2}$. In their results, the value of a is higher for a more viscous liquid, which means that the retreating speed of the jet can be affected by viscosity. As the capillary speed (v_{ca}) does not include a viscosity term, it is necessary to relate the liquid viscosity to the retreating speed using other characteristic parameter.

Recently Brenner et al. [27] showed the shape of the thread end of a viscous film can remain flat rather than being collected into a rim due to a viscous effect when

$$Re_f = \frac{U_0 L_f}{\nu} < 1, \quad (6)$$

where ν is the kinematic viscosity, U_0 the retraction speed, L_f the axial extent of the film and is the Reynolds number based on these parameters. In addition to Re_f, the square of the Ohnesorge number, $Oh^2=\mu^2/(\gamma\rho R)$ is another dimensionless parameter employed to determine the shape of the retracting film edge. While Re_f determines whether the rim is round or not, this parameter shows the relative dominance between the growth of capillary waves on the thread and the retraction of the film [27]. As a different shape of the thread end can change the retreating dynamics of a liquid thread, the parameters can be useful in relating the viscous effect to jet retraction (i.e., jet tail speed). Thus, in this experiment, the viscous effect is discussed by comparing two parameters, Re_j and Oh^2, which are also represented by $v_t L_0/\nu$ and $\mu^2/(\gamma\rho R_{noz})$, respectively. Characteristic length, L_0, used in this parameter is called initial thread length, which is the length of the jet thread at the instance of the jet pinch-off from the nozzle. The parameters of different viscous liquids at different pulse amplitudes are given in Table 2.

In the table, the ratio of jet tail speed (v_t) and capillary speed (v_{ca}) increases for a more viscous liquid, which corresponds to the results of Dong et al. [23]. It means that the capillary speed (v_{ca}) is insufficient to explain the fast jet tail speed for a more viscous liquid as explained above. Assuming their surface tension is the same, the difference of the retraction speed must come from the shape of the jet thread. Brenner et al. [27] compared the shape of the retracting viscous film by simulation, and showed that the shape of the retracting film becomes flat at higher L_v/R_{noz} and lower Re_f. Here, L_v/R_{noz} is the aspect ratio that designates the dimensionless parameter Oh^2. Brenner et al. [27] gave a definition of 'l_v/e' as a '$\eta^2/(\gamma\rho e)$'. In our experiment, the value of L_v/R_{noz} increased and Re_j decreased for more viscous liquids, which favorably makes the shape of the jet thread to be more sharp and conical at the tail edge, as can be seen in Fig. 6. In addition, in the case of the glycerol 20 wt% solution, the neck of the thread near the primary drop rapidly necks down compared with the glycerol 60 wt% solution, which makes the pressure profile inside the thread unfavorable to jet retraction. The delay of the neck-down for the glycerol 60 wt% solution is because the propagation of capillary wave in the thread is resisted by the enhanced viscosity. Thus the surface energy is dissipated by retracting the thread into a primary drop rather than breaking up into satellites. It finally results in the increase of the retraction speed.

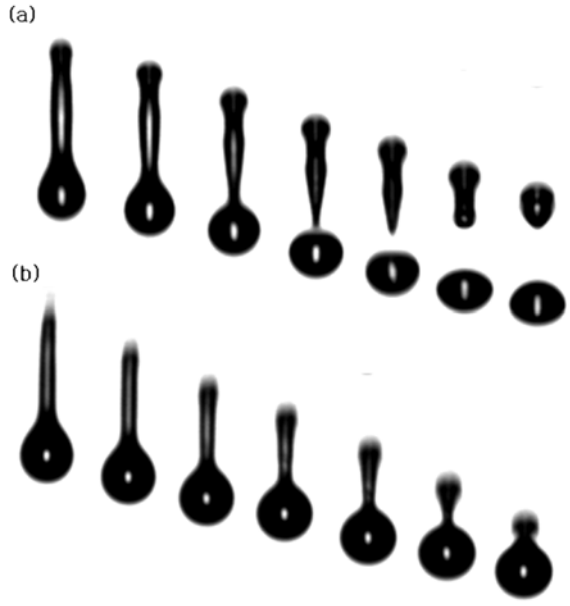

Fig. 6. The shape of retracting liquid thread at the same jet length. The sequential pictures of liquid thread were taken every 2 μs: (a) glycerol 20 wt% solution at pulse amplitude 30 V, (b) glycerol 60 wt% solution at pulse amplitude 32 V.

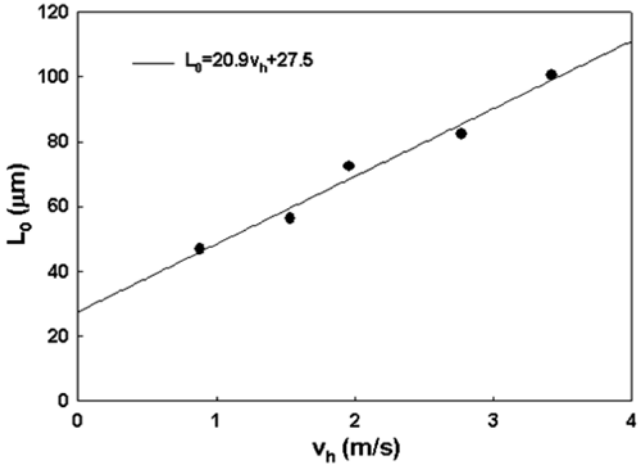

Fig. 7. Linear relationship between initial thread length and jet head speed for DI water.

2. Calculation of Jet Retraction Time

The initial thread length (L_0) is defined as the length of the liquid thread, which is the jet length (L) subtracted by the diameter of the primary drop when it is detached from the nozzle. In most cases, the initial thread length is the maximum thread length because the retraction begins after the detachment. The initial thread length depends on jet head speed (v_h) as was seen in Table 2. In Fig. 7, it can be recognized that these two variables have a linear relationship. Thus, it is possible to estimate the initial thread length from the jet head speed (v_h) by the following fitting equation:

$$L_0 = k_1 \cdot v_h + k_2, \tag{7}$$

where k_1, k_2 are fitting parameters.

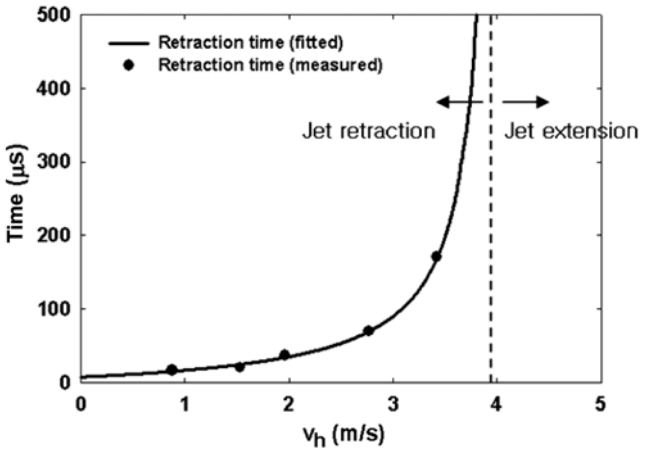

Fig. 8. The time necessary for the retracting tail of the jet to reach its head. The curve diverges when the jet head speed (v_h) equals the jet tail speed (v_t), near 4 m/s for DI water. The jet thread extends further without retraction beyond this point.

The jet retraction time (t_r) is now defined as the total time necessary for the tail end to reach the drop head without a break-up. The retraction time can be obtained from

$$t_r = \frac{L_0}{v_r} = \frac{k_1 v_h + k_2}{v_r}. \tag{8}$$

As the retraction speed (v_r) is the difference between the jet head speed and tail speed ($v_t - v_h$), it becomes

$$t_r = \frac{k_1 v_h + k_2}{v_t - v_h}. \tag{9}$$

Using this Eq. (9), the retraction time can be calculated as a function of jet head speed (v_h) because the jet tail speed (v_t) is considered to be constant at different pulse amplitudes (i.e., at different v_h) as explained before. The plot of Eq. (9) is shown in Fig. 8. To obtain the graph, the average value of v_t at different pulse amplitudes in Table 2 was used.

In the figure, the retraction time has a minimum at zero jet head speed and diverges to infinity at a critical jet head speed (v_t), beyond which ($v_h > v_t$) jet extension occurs rather than retraction because the jet head speed becomes higher than the speed of the tail end. If the drop breaks up into satellites under this condition, the disintegrated drops cannot recombine with each other. So it can be used as a guideline to predict whether the primary drop and its satellites recombine or not.

3. Measurement of Jet Break-up Time

The jet break-up time (t_b) is defined as the time interval between the jet pinch-off at the nozzle (t_0) and the drop pinch-off at the neck of the primary drop (t_1) (Fig. 4b). The jet break-up time slightly depends on pulse amplitude, but the variation is not significant compared to the retraction time [Table 3]. Dong et al. [23] showed that two pinch-off times (t_0, t_1) vary little with voltage, ejection speed and initial thread length based on linear stability analysis [28]. From the linear stability analysis, the time at which the liquid is broken up by the fastest growing capillary wave is approximated by

$$t_{break}=\frac{1}{\alpha^*_{max}}\left(\frac{\rho R^3_{noz}}{\gamma}\right)^{1/2}\ln\left(\frac{R_{noz}}{\varepsilon_{max}}\right)=C\frac{t_{ca}}{\alpha^*_{max}}, \quad (10)$$

where $C=\ln(R_{noz}/\varepsilon_{max})$ and $t_{ca}=(\rho R^3_{noz}/\gamma)^{1/2}$ is the capillary time, ε_{max} is the initial amplitude of the capillary wave disturbance. And α^*_{max} is the fastest growth rate of capillary wave, which is expressed by

$$\alpha^*_{max}=\left(\left[\frac{1}{2}x^2_{max}(1-x^2_{max})+\frac{9}{4}Oh^2x^4_{max}\right]^{1/2}-\frac{3}{2}Ohx^2_{max}\right), \quad (11)$$

where $Oh=\mu/\sqrt{\rho R_{noz}\gamma}$ is the Ohnesorge number and x_{max} is the fastest growth mode. It is again approximated by

$$x_{max}=\frac{1}{2+\sqrt{18}Oh}. \quad (12)$$

To use the equations in calculating the two break-up times, t_0 and t_1, Dong et al. [23] assumed that they are determined by the most unstable disturbance. Then, it is possible to express the jet break-up time (t_b) which is simplified to

$$t_b=t_1-t_0=(C_1-C_0)\frac{t_{ca}}{\alpha^*_{max}}=C^*\frac{t_{ca}}{\alpha^*_{max}}. \quad (13)$$

In Table 3, the calculated t_{ca}, α^*_{max}, C^* for different liquid samples are tabulated. According to Dong et al. [23], C^* should be in the range of 0.2 and 0.4, and our experimental data show a good accordance with them even though the value is slightly exceeded for the glycerol 60 wt% solution. This means that the assumption they made is acceptable in interpreting the jet break-up phenomenon. Thus, we come to the conclusion that the jet break-up time variation at different pulse amplitudes is negligible in accordance with Dong et al. [23], and it can be considered constant for the same material. It enables us to use the averaged value of the break-up times measured at different pulse amplitudes in representing the break up time of a material.

4. Stability of Liquid Thread

A more viscous liquid can resist the drop break-up more than a less viscous liquid. This causes a different jet behavior among different viscous samples, especially with respect to the satellite drop formation. In Fig. 9, for example, glycerol 60 wt% solution forms much fewer satellite drops than other fluids.

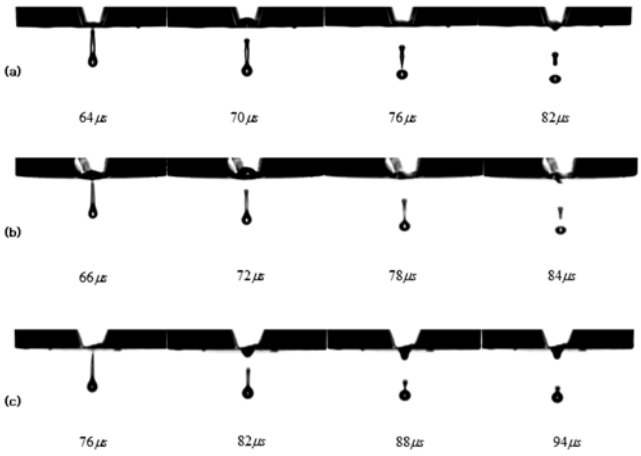

Fig. 9. Jetting behavior of different viscous fluids at pulse amplitude 33 V: (a) glycerol 20 wt%, (b) glycerol 40 wt%, and (c) glycerol 60 wt%.

To estimate the jet stability in terms of the satellite generation, a jetting window can be drawn in terms of processing parameters, pulse amplitude and dwell time, as shown in Fig. 10. The figure indicates whether the satellite is formed or not at different processing conditions. It can be observed that the region of stable drop formation increases as the viscosity increases.

The jetting window graph enables us to estimate jettable condition and the degree of jet break-up. To describe the jet stability more quantitatively, two characteristic times, retraction time and break-up time of the jet thread, need to be considered. By putting both the retraction time and the break-up time on the same plot, the jet stability graph can be obtained. A typical shape of a jet stability graph is shown in Fig. 11.

In the graph, the two vertical dashed lines indicate the critical jet speeds. The upper critical jet speed ($v_{c,upper}$) is the jet head speed (v_h) where the retraction time becomes diverging, and it equals the jet tail speed (v_t), as explained before. The jet head speed where

Table 3. Break-up time, capillary time, Ohnesorge number and parameters to determine the characteristics of capillary jet break-up

Liquid	Voltage (V)	t_b (μs)	t_{ca} (μs)	Oh	x^2_{max}	α^*_{max}	C^*
DI water	25	10.5	14.7	0.024	0.48	0.34	0.24
	27	10.5					0.24
	30	9.5					0.22
	33	14					0.32
	36	15					0.34
Glycerol 20 wt%	27	11.5	15.5	0.066	0.44	0.31	0.23
	30	13.5					0.27
	33	14.5					0.29
	36	13.0					0.26
Glycerol 40 wt%	30	15.0	16.1	0.11	0.41	0.29	0.27
	33	16.5					0.29
	36	17.0					0.30
Glycerol 60 wt%	33	26	16.8	0.25	0.33	0.23	0.36
	36	30					0.41
	39	31					0.43

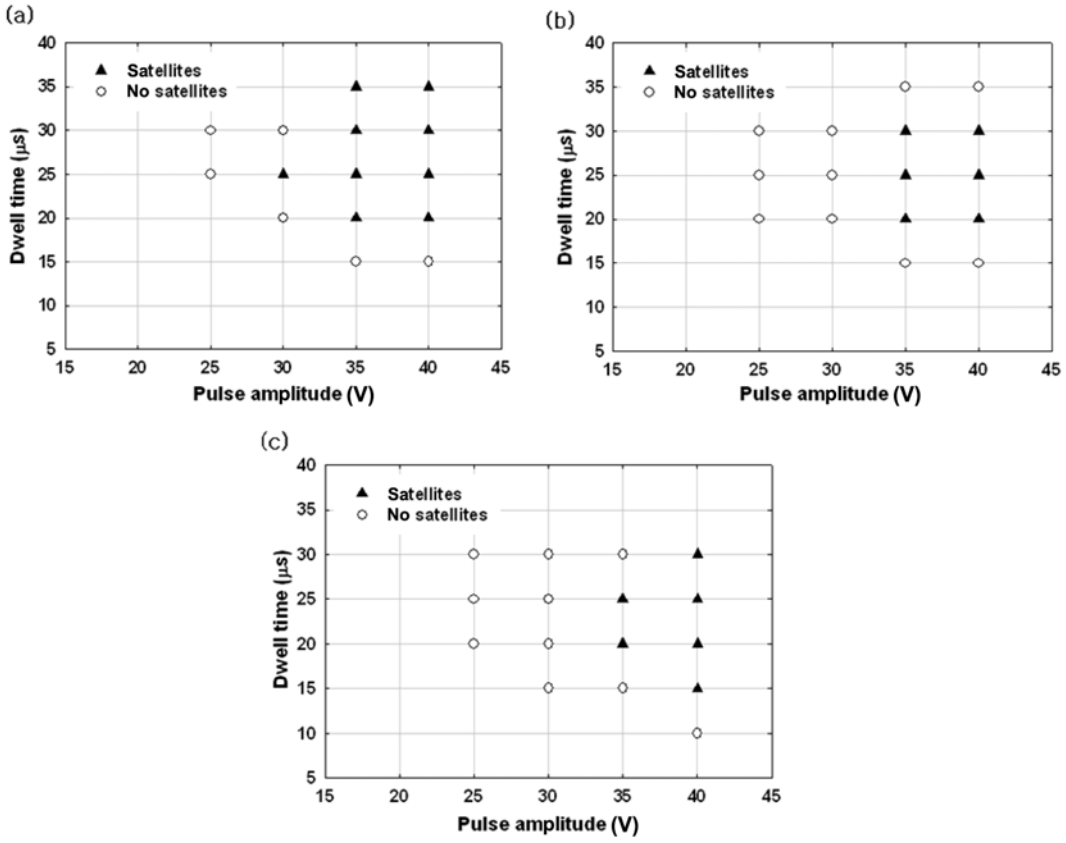

Fig. 10. Jetting window graph: (a) glycerol 20 wt% solution, (b) glycerol 40 wt% solution, and (c) glycerol 60 wt% solution.

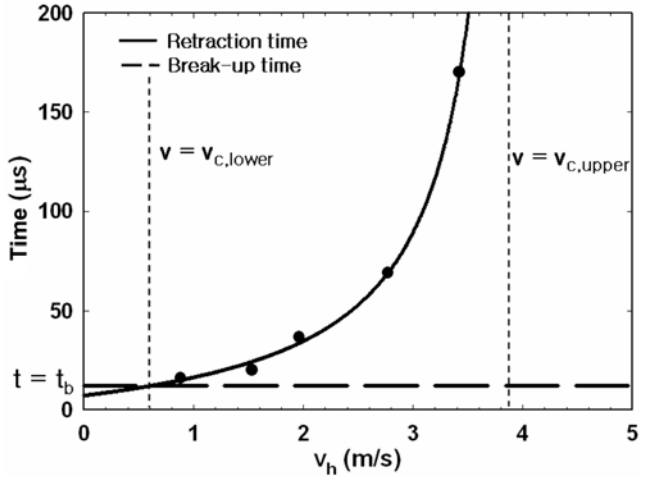

Fig. 11. Typical shape of jet stability graph (DI water). The retraction time curve (solid line) meets break-up time curve (dashed line) at 0.6 m/s (lower critical speed), and diverges at around 3.8 m/s (upper critical speed). Average break-up time (t_b) of DI water was calculated 19 μs in the experiment.

the retraction time equals the average break-up time is called the lower critical jet speed ($v_{c,lower}$). It can be calculated from

$$t_r = \frac{k_1 v_{c,lower} + k_2}{v_t - v_{c,lower}} = t_b, \tag{14}$$

$$v_{c,lower} = \frac{v_t t_b - k_2}{k_1 + t_b}. \tag{15}$$

Regarding the critical speeds, the expected jet break-up behavior can be divided into three parts:

(i) $v_h < v_{c,lower}$: Retraction time is shorter than the break-up time. Liquid thread is retracted without a break-up.

(ii) $v_{c,lower} < v_h < v_{c,upper}$: Break-up time is shorter than the retraction time. Pinch-off at the neck of the liquid thread is observed. But the separated drop can be merged into the primary drop.

(iii) $v_h > v_{c,upper}$: Jet extension occurs. The separated drop does not merge into the primary drop.

The jet stability graphs for different viscous liquids are shown in Fig. 12. The viscous effect on both the retraction time and the break-up time is clearly observed. In Fig. 12d, the two critical parameters, $v_{c,upper}$ and $v_{c,lower}$, are plotted against the viscosity. They increase as the viscosity increases, which means an enhanced jetting stability. The reason for this improvement was already explained by two factors: the faster drop retraction and the longer break-up time. In terms of the suppression of the satellite drops, it is noteworthy that the increase of the lower critical speed ($v_{c,lower}$) gives a possibility for satellites to recombine up to the more severe conditions like high pulse amplitude and the upper critical speed ($v_{c,upper}$) associated with the jet retraction property. In other words, the two boundary conditions are applicable to the judgment of the jetting property in the controlled processing parameters. Thus, it can be said that the effect of shear viscosity is successfully characterized by this stability graph when we focus on the satellite generation and its recombination.

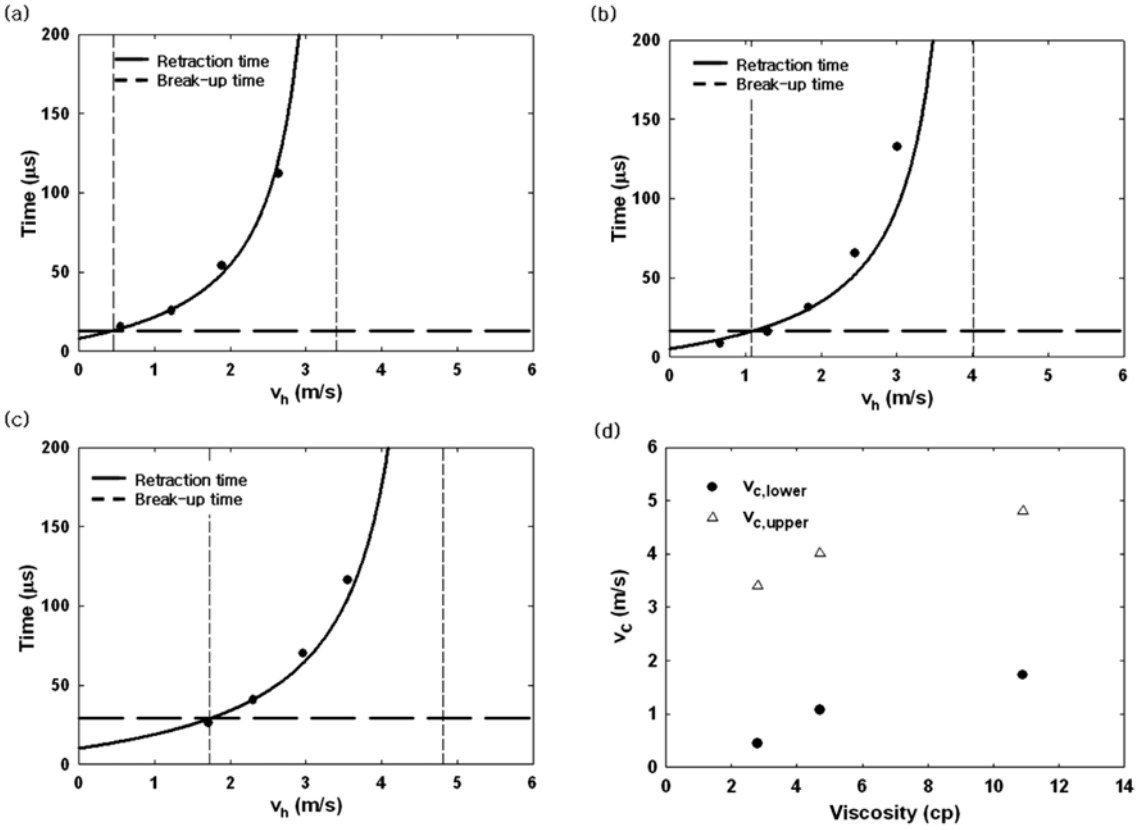

Fig. 12. Jet stability graph of different fluids. An increase of lower and upper critical speeds is observed for more viscous liquids: (a) glycerol 20 wt% solution, (b) glycerol 40 wt% solution, (c) glycerol 60 wt% solution. (d) critical jet speed vs. viscosity of the samples.

Extensional viscosity is also an important factor, but the low viscosity range (1.0-11 cp) of our prepared fluids is inadequate to measure it even by using CaBER (capillary breakup extensional rheometer).

In addition, the approach appears useful in predicting the jet stability of non-Newtonian liquids through the preliminary tests. Details of the non-Newtonian behavior will be reported later.

5. Effect of Dwell Time (Pulse Width)

The pulse shape of the waveform used to excite a piezoelectric transducer inside the nozzle has a critical effect on the drop ejection [5,18]. With the single-peak electric pulse, by tuning the pulse width, it is possible to get the optimal condition for the stable drop formation. In a DOD jetting system, the energy generated by a piezoceramic actuator is transferred to the nozzle end. This is due to the boundary conditions of both ends as a fixed closed end at the orifice and an open end at the fluid supply. Therefore, to explain the energy transfer between the actuator and the nozzle, the generation of a pressure wave and its propagation in the liquid must be considered. Bogy and Talke [17] proposed the propagation theory to explain the dwell time effect with simplified the inkjet head unit as in Fig. 13.

In the experiment, when we change the dwell time at the pulse amplitude 30 V, three different jettable regimes can be observed. They are shown in Fig. 14a. The dwell time corresponding to the maximum jet head speed (v_h) is regarded as the optimal dwell time because the fastest jet can be made only when the internal pressure is highly amplified by a resonance.

Using the propagation theory [17], the first optimal dwell time t_{opt} can be calculated. If the length of the printhead is L_p (Fig. 13),

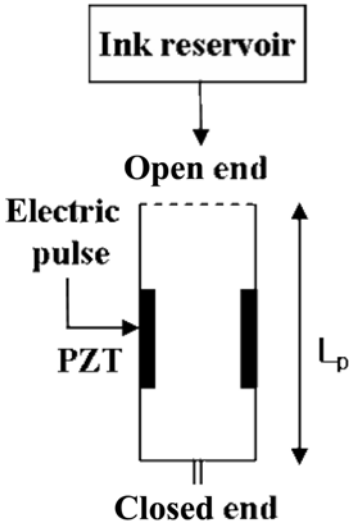

Fig. 13. Cross sectional schematic diagram of inkjet head for propagation theory. The geometry of the printhead tube is simplified by a cylinder, and one side of the cylinder connected to the ink reservoir is regarded open while the other side connected to the nozzle is regarded closed due to very small size of the nozzle.

the first resonance inside the nozzle occurs when a split pulse wave travels the distance L_p. To confirm the validity of this theory in predicting the first optimal dwell time, DI water was tested. As the speed

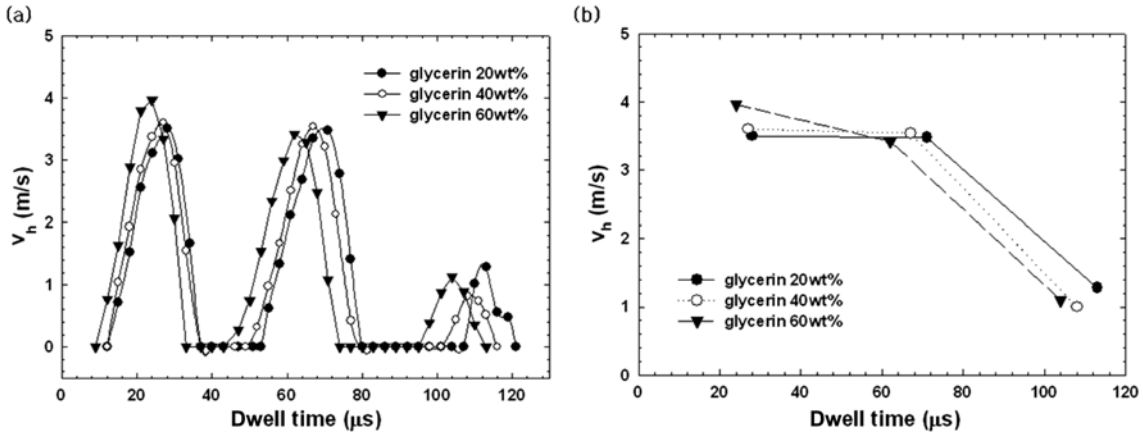

Fig. 14. Jet speed variation as a function of dwell time at pulse amplitude 30 V and frequency 500 Hz: (a) three different jetting regimes for different viscous fluids, (b) jet head speed at optimal dwell time.

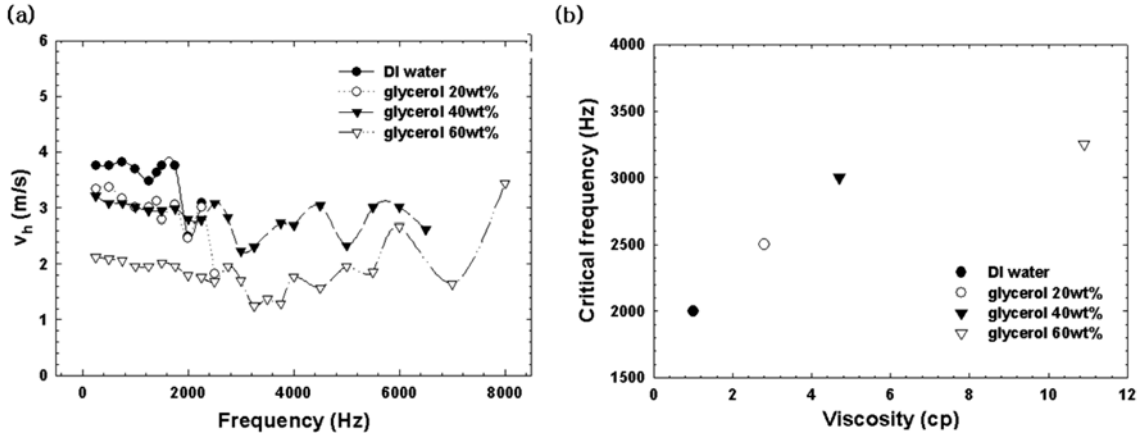

Fig. 15. Effect of pulse frequency. Jet speed variation is measured at several different frequencies at fixed pulse amplitude (30 V) and dwell time (30 μs): (a) jet speed variation as a function of frequency, (b) critical frequency for different viscous liquids.

of an acoustic wave in the DI water ($v_{aco,water}$) is about 1,435 m/s [12], the first optimal dwell time can be calculated according to the following equation:

$$t_{opt,water} = \frac{L_p}{v_{aco,water}} = \frac{15(\text{mm})}{1435(\text{m/x})} \approx 10.5(\mu\text{s}). \quad (16)$$

Due to the rising time and falling time of the pulse, the first optimal dwell time can be slightly higher than 10.5 μs. We obtained 10 μs of the optimal dwell time of DI water. It still shows good agreement in time scale with the measured one.

The viscous effect on the optimal dwell time can also be explained by the propagation theory. In Fig. 14b, the jet head speed (v_h) of each sample at the three optimal dwell times is plotted. The more viscous the liquid, the shorter the optimal dwell time. For example, the glycerol 60 wt% solution has almost 10 μs lower optimal dwell time than the glycerol 20 wt% solution. The shift of t_{opt} is affected by the different acoustic wave speed (v_{aco}). In general, the acoustic wave becomes fast in a more viscous medium, which makes the t_{opt} value smaller in Eq. (16).

6. Effect of Frequency

In order to achieve an accurate drop placement, it is desirable that all the drops ejected from the multi-nozzle printhead have the same velocity, independent of the frequency [19].

In Fig. 15a, the frequency dependence of jet head speed (v_h) is shown for different viscous samples. There exists a certain frequency over which the jet head speed becomes unstable and oscillating. For the DI water, the first rapid drop in the jet speed occurs at 2,000 Hz. To compare the effect of the viscosity more clearly, the critical frequency was defined as the maximum frequency before the variation of jet head speed more than 30% of the initial speed. The critical frequencies for different viscous samples are plotted in Fig. 15b. The sample with the higher viscosity delays the onset of the jet speed variation up to the higher frequency. This instability of jet speed at high frequency is caused by the remaining acoustic waves. Even after a drop is ejected, there remain acoustic waves inside the nozzle due to the reflection of the pressure wave at the nozzle ends. This remaining wave continuously travels along the printhead tube until it is totally annihilated by energy dissipation. At high frequency, the remaining wave comes to interfere with the newly formed pulse wave and then the drop formation becomes unstable. A more viscous fluid loses more energy than a less viscous fluid through viscous dissipation, and can generate consistent drops up to the higher fre-

quency without being interfered by the remaining waves.

CONCLUSIONS

A method for practically evaluating the jet stability of DOD inkjet printing in terms of satellite drop generation has been proposed. The method was first applied by measuring the relative stability of liquids with a different shear viscosity but of a comparable surface tension. Comparing two characteristic times (retraction time, break-up time), the increase of the jet stability for more viscous liquids was successfully quantified by the increase of upper and lower critical jet speeds. In addition to the jetting stability, the effect of two important variables, the dwell time and the frequency, which determine the imposed electric pulse shape on PZT, were studied as well. For a glycerol and water mixture, there existed three jettable dwell time regions and the optimal dwell time decreased for more viscous liquids. The critical frequency which is the maximum stable frequency without a significant change in the jet speed, was observed for different viscous liquids. It was found that a more viscous liquid is stable up to a higher frequency because high viscosity can extinguish the remaining wave pulse inside the nozzle more easily through energy dissipation. As the method was designed to be used for a wider range of inks, including complex fluids, it can be applied to any ink including polymers and particles. The application to such a complex fluid system will soon be reported.

ACKNOWLEDGMENT

This work was supported by the National Research Laboratory Fund (M10300000159) of the Ministry of Science and Technology in Korea.

REFERENCES

1. B. D. Gans, P. C. Duineveld and U. S. Schubert, *Macromole. Rapid Commun.*, **24**, 659 (2003).
2. P. Calvert, *Chem. Mater.*, **13**, 3299 (2001).
3. H. Sirringhaus, T. Kawase, R. H. Friend, T. Shimoda, M. Inbasekaran, W. Wu and E. P. Woo, *Science*, **290**, 2123 (2000).
4. T. Kawase, H. Sirringhaus, R. H. Friend and T. Shimoda, *Adv. Mater.*, **13**, 1601 (2001).
5. J. B. Szczech, C. M. Megaridis, D. R. Gamota and J. Zhang, *IEEE Transactions on Electronics Packaging Manufacturing*, **25**, 26 (2005).
6. B. D. Gans, P. C. Duineveld and U. S. Schubert, *Adv. Mater.*, **16**, 203 (2004).
7. R. P. Mun, J. A. Byars and D. V. Boger, *J. Non-Newtonian Fluid Mech.*, **74**, 285 (1998).
8. Y. Christanti and L. M. Walker, *J. Non-Newtonian Fluid Mech.*, **100**, 9 (2001).
9. Y. Christanti and L. M. Walker, *J. Rheol.*, **46**, 733 (2002).
10. J. J. Copper-White, J. E. Fagan, V. Tirtaatmadja, D. R. Lester and D. V. Boger, *J. Non-Newtonian Fluid Mech.*, **106**, 29 (2002).
11. T. M. Liou, K. C. Shih, S. W. Chan and S. C. Chen, *Int. Comm. Heat Mass Transfer*, **29**, 1109 (2002).
12. H. C. Wu, W. S. Hwang and H. J. Lin, *Mater. Sci and Eng.*, **A373**, 268 (2004).
13. H. C. Wu, W. S. Hwang and H. J. Lin, *Modelling Simul. Mater. Sci. Eng.*, **13**, (2005).
14. J. E. Fromm, *IBM J. Res.*, **28**, 322 (1984).
15. D. Y. Shin, P. Grassia and B. Derby, *Int. J. Mech. Sci.*, **46**, 181 (2004).
16. T. W. Shield, D. B. Bogy and F. E. Talke, *IBM J. Res.*, **31**, 96 (1987).
17. D. B. Bogy and F. E. Talke, *IBM J. Res.*, **28**, 307 (1984).
18. H. C. Wu, T. R. Shan, W. S. Hwang and H. J. Lin, *Mater. Transactions*, **45**, 1794 (2004).
19. F. C. Lee, R. N. Mills and F. E. Talke, *IBM J. Res.*, **28**, 307 (1984).
20. W. W. Carr and J. F. Morris, *Nat. Textile Center Annual Report* (2003).
21. W. W. Carr, H. Park and D. Bucknall, *Nat. Textile Center Annual Report* (2005).
22. H. J. Shore and G. M. Harrison, *Phys. Fluids*, **17**, 033104 (2005).
23. H. Dong, W. W. Carr and J. F. Morris, *Phys. Fluids*, **18**, 072102 (2006).
24. G. I. Talyer, *Proc. R. Soc. London*, Ser **A253**, 313 (1959).
25. J. B. Keller, *Phys. Fluids*, **26**, 3451 (1983).
26. F. E. C. Culick, *J. Appl. Phys.*, **31**, 1128 (1960).
27. M. P. Brenner and D. Gueyffier, *Phys. Fluids*, **11**, 737 (1999).
28. J. Eggers, *Rev. Mod. Phys.*, **69**, 865 (1997).